J. Fluid Mech. (1995), vol. 303, pp. 279–295

A numerical model of the hydrodynamics of the thermal bar

By DUNCAN E. FARROW

School of Mathematics, University of East Anglia, Norwich NR4 7TJ, UK

(Received 16 January 1995 and in revised form 4 August 1995)

The thermal bar phenomenon is modelled numerically by the natural convection of a fluid contained in a two-dimensional triangular domain. The non-rotating case considered here is appropriate to laboratory models of the thermal bar. Three sets of results are presented reflecting varying degrees of nonlinearity. The results are discussed in relation to available theoretical and experimental results.

1. Introduction

At the end of winter, the water temperature in many temperate lakes is less than 4°C, the temperature at which water achieves its maximum density. As the spring warming proceeds, the shallow nearshore waters heat more rapidly than the deeper parts. As a consequence, the 4°C isotherm propagates out from the shore and to either side of it the horizontal pressure gradient has opposite signs. This leads to a double-cell circulation pattern with downwelling in the vicinity of the 4°C isotherm. This isotherm is called the thermal bar and inhibits horizontal transport from the shallows to the deeper parts of the lake. A similar phenomenon occurs at the end of autumn as the lake waters are cooled towards 4°C. The shallow waters cool more rapidly and because of the symmetry of the density relation about 4°C, a circulation pattern develops which is similar to that occurring at the end of winter.

The thermal bar has been the subject of a number of field experiments. Malm *et al.* (1993) report temperature and current measurements made during the spring 1991 thermal bar event in Lake Ladoga. The main results are that the isotherms were nearly vertical throughout the study region and there is a significant amount of horizontal heat transport from the warmer nearshore waters into the thermal bar region. The vertical isotherms throughout the study region are in contrast to the results of other field studies (for example, Hubbard & Spain 1973 or Malm *et al.* 1994) which show a stably stratified region on the warmer nearshore side of the thermal bar. The vertical isotherms observed by Malm *et al.* (1993) are due to the significant amount of wind-induced vertical mixing. The vertical mixing led to the approximately spatially uniform surface heat flux being distributed approximately uniformly over the local depth. This, combined with the variable topography, led to nearly vertical isotherms. Malm *et al.* (1993) also observed a complex, largely wind-driven, circulation pattern. In the above field experiments it was found that the circulation associated with the thermal bar was dominated by Coriolis effects.

There have been a number of theoretical and numerical studies of the thermal bar in the rotating frame. Huang (1972) derived an asymptotic solution (based on small Rossby number) for the steady-state temperature and circulation pattern in

Lake Michigan. He found general agreement between his results and available field measurements of Lake Michigan. Bennett (1971) numerically studied an idealized model for the thermal bar. In his hydrostatic model, there was no variation in the longshore direction though Coriolis effects were included. He found that the flow was generally in geostrophic balance, with longshore velocities being generally an order of magnitude greater than offshore velocities. Malm & Zilitinkevich (1994) calculated the circulation in a convectively mixed (temperature independent of depth) lake. Their steady linear solutions were in qualitative agreement with field observations. More recently, Malm (1994) numerically modelled the circulation associated with the thermal bar. Malm's model was similar to Bennett's (1971) model with the principal difference being that Malm's model was not hydrostatic. Malm also considered the effect of wind on the circulation.

The thermal bar in the non-rotating frame (which is the focus of this paper) has been studied experimentally by Elliott & Elliott (1969, 1970) and Kreyman (1989). Despite the absence of Coriolis effects, those experiments were able to reproduce in the laboratory many of the features of the thermal bar observed in the field. In those experiments, water at less than 4°C contained in a shallow triangular tank was heated from above. In Elliott & Elliott's experiments, the heating was via infra-red lamps which meant that most of the heat input occurred in the top 1 or 2 cm of the 13 cm deep tank. This led to a strongly stratified warm region in the shallow end of the tank behind the thermal bar and a vertically well-mixed cold region ahead of the thermal bar. This is very similar to the structure observed in Lake Superior by Hubbard & Spain (1973). The surface heating in Kreyman's (1989) experiments was via lamps with most of their heat in the visible spectrum. This meant that the heat penetrated deeper into the water and led to a weaker stratification in the shallows than that observed by Elliott & Elliott.

Many theoretical studies of the thermal bar in the non-rotating frame have concentrated on modelling the heat balance associated with the propagation of the thermal bar. In conjunction with their experimental work, Elliott & Elliott (1970) developed a two-dimensional model which neglected the horizontal transport of heat. By distributing a surface heat flux over the local depth and balancing this against the rate of increase of temperature, Elliott & Elliott concluded that the thermal bar would move out from the shore at a constant speed given by

$$\text{propagation speed} = I_0/(\rho_0 C_p A(T_m - T_0)) \tag{1.1}$$

where I_0 is the surface heat flux, ρ_0 is the reference density, C_p is the specific heat of water, T_0 is the initial temperature of the water, T_m is the temperature at which the density maximum occurs and A is the bottom slope. Note that the propagation speed is constant only if all the parameters on the right-hand side of (1.1) are constant. Elliott & Elliott found general agreement with their experiments except that the propagation of the thermal bar seemed to have two distinct phases; an initial 'slow' phase where it moved out more slowly than predicted and a later 'fast' stage where it moved out more rapidly than predicted. A similar two-phase propagation was noted by Kreyman (1989). Zilitinkevich, Kreiman & Terzhevik (1992) describe a more complex heat balance model that allows for the horizontal transport of heat from the warm shallow regions into the vicinity of the thermal bar thereby increasing its propagation speed. This more complex heat balance model was able to reproduce the 'fast' phase of the thermal bar's propagation. Elliott (1970) developed a model for the circulation associated with the thermal bar by assuming a balance between vertical shear and the horizontal pressure gradient. In that model, the flow was driven by an

unsteady temperature field derived from a one-dimensional (in the vertical) diffusion equation with a surface heat flux. Elliott found reasonable agreement between his results and the experimental results of Elliott & Elliott (1969, 1970). However, the spin-up time scale based on the depth of the experimental tank and molecular values for viscosity suggests that a viscous/buoyancy balance would not be achieved in the entire tank before the experiment ended and that inertial effects, particularly in the deeper parts of the tank, could be important. Farrow (1995, hereafter referred to as I) presented an asymptotic solution (based on small bottom slope) for an idealized model for the thermal bar phenomenon in the non-rotating frame that included inertial effects. One of the results of that work is that inertial effects lead to a slower propagation speed for the thermal bar than those predicted by previous heat-balance-based estimates. In that work, the thermal bar and the point on the surface where the downwelling occurs are distinct features and can be separated by an arbitrarily large distance.

In a departure from the heat balance or general circulation models, Kay, Kuiken & Merkin (1995) examined the detail of the downwelling region of the thermal bar. They modelled this region as a sinking plume of water at temperatures near the density maximum. Their steady-state boundary layer analysis yielded the vertical velocity and temperature structure in the plume as well as the horizontal velocity induced in the far field.

All the above models of the non-rotating case involve some simplification of the dynamics, for example by assuming that steady-state conditions prevail or by ignoring nonlinear effects. This paper presents unsteady numerical solutions of a two-dimensional model of the thermal bar system in the non-rotating frame. The model formulation follows very closely that described in I with a vertically uniform heating term being an important feature. The aim of the current work is to confirm the validity of the asymptotic solution of I as an approximate solution to the full model as well as to examine flows in the parameter range where the asymptotic solutions break down. The results will be discussed in terms of available theoretical and experimental results.

2. Model formulation

The model formulation follows very closely that described in I with the main difference being that the governing equations are written in polar rather than Cartesian coordinates. There are numerical advantages in having the physical boundaries lying on coordinate lines. In I, the spring thermal bar is modelled by the natural convection of a fluid lying in the region bounded by the lines $z = 0$ and $z = -Ax$ in the (x, z)-plane where A is the slope of the bottom boundary. In terms of (r, θ)-coordinates, the boundaries are $\theta = 0$ and $\theta = -\tan^{-1} A$. The flow in this region is driven by an internal heat source term Q in the heat conservation equation derived by distributing a spatially uniform surface heat flux of I_0 Wm^{-2} uniformly over the local depth. Thus, the heat conservation equation is

$$\frac{\mathrm{D}T}{\mathrm{D}t} = \kappa \nabla^2 T + \frac{I_0}{\rho_0 C_p A x} \tag{2.1}$$

where ρ_0 is the reference density, C_p is the specific heat of water and κ is the thermal diffusivity. The heat source term is inversely proportional to the distance from the shore which gives rise to horizontal temperature gradients that drive the flow.

The nonlinear relationship between the density ρ and the temperature T is of

primary importance for the thermal bar phenomenon. For this work, it is assumed to take the form

$$\rho - \rho_0 = \rho_0 \frac{a_1 \Delta T - a_2 \Delta T^2}{1 + b\Delta T} \tag{2.2}$$

where $\rho_0 = \rho(T_0)$, $\Delta T = T - T_0$ and (a_1, a_2, b) are all parameters that depend on the reference temperature T_0. The above form for $\rho(T)$ is identical to that described in I and is obtained by truncating the representation found in Appendix F of Gebhart *et al.* (1988). The above form captures the linear behaviour for small and large T as well as the quadratic behaviour near the density maximum.

Neither the geometry of the flow domain (which is semi-infinite in the idealized model of I) nor the nature of the forcing suggest any natural length scales. Length and time scales are derived in the present case by balancing two length scales that evolve differently with time. The first is a scale for the distance over which viscous effects will be felt in a time t: $\delta = (\nu t)^{1/2}$, where ν is the kinematic viscosity. For the second length scale, suppose that the fluid is initially at some temperature $T = T_0$. Balancing the heat source and unsteady terms in (2.1) yields a scale for the temperature change that depends on t:

$$T - T_0 \sim I_0 t/(\rho_0 C_p A x). \tag{2.3}$$

The horizontal position at which $T = T_m$ (where T_m is some specified temperature) is given by

$$x_m \sim I_0 t/((T_m - T_0)\rho_0 C_p A) \tag{2.4}$$

where the local depth will be $h_m = A x_m$. Note that the above argument is equivalent to Elliott & Elliott's (1970) work and immediately leads to the thermal bar propagation speed given by (1.1). Identifying h_m with δ yields a vertical length scale h and a time scale τ:

$$h = \nu a_1 \rho_0 C_p/(2a_2 I_0), \tag{2.5}$$

$$\tau = \nu \left(a_1 \rho_0 C_p/(2a_2 I_0)\right)^2 \tag{2.6}$$

where T_m has been chosen so that the numerator of (2.2) is at its maximum. In practice, T_m is very close to the maximum density temperature. For consistency with the asymptotic results of I, θ is scaled with A.

Radial and tangential velocity scales are derived by assuming a viscous/buoyancy balance, from which

$$u \sim U = AGrh/\tau, \tag{2.7}$$

$$w \sim AU \tag{2.8}$$

where Gr is the Grashof number of the model,

$$Gr = g\Delta\rho_0 h^3/\rho_0 \nu^2 \tag{2.9}$$

where $\Delta\rho_0 = \rho_0 a_1^2/2a_2$ is a scale for the density perturbation. A scale for the pressure perturbation is obtained via a hydrostatic balance $p \sim gh\Delta\rho_0$.

The dimensionless Boussinesq equations governing the flow are then

$$\frac{\partial u}{\partial t} + A^2 Gr\left(u\frac{\partial u}{\partial r} + \frac{1}{r}w\frac{\partial u}{\partial \theta} - A^2\frac{1}{r}w^2\right) = -\frac{\partial p}{\partial r} + A^2\frac{1}{r}\frac{\partial}{\partial r}\left(r\frac{\partial u}{\partial r}\right) + \frac{1}{r^2}\frac{\partial^2 u}{\partial \theta^2} - A^2\frac{2}{r^2}\frac{\partial w}{\partial \theta} - A^2\frac{1}{r^2}u - \frac{1}{A}\sin(A\theta)\frac{T - T^2/2}{1 + \gamma T}, \tag{2.10}$$

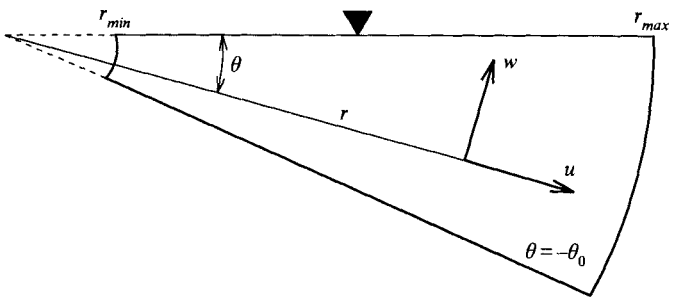

FIGURE 1. Schematic of the computational flow domain and the coordinate system with the origin at the tip of the wedge. The solid triangle indicates the position of the fluid surface.

$$\frac{\partial w}{\partial t} + A^2 Gr\left(u\frac{\partial w}{\partial r} + \frac{1}{r}w\frac{\partial w}{\partial \theta} + \frac{1}{r}wu\right) = -\frac{1}{rA^2}\frac{\partial p}{\partial \theta} + A^2\frac{1}{r}\frac{\partial}{\partial r}\left(r\frac{\partial w}{\partial r}\right) + \frac{1}{r^2}\frac{\partial^2 w}{\partial \theta^2} + A^2\frac{2}{r^2}\frac{\partial u}{\partial \theta} - A^2\frac{1}{r^2}w - \frac{1}{A^2}\cos(A\theta)\frac{T - T^2/2}{1+\gamma T}, \tag{2.11}$$

$$\frac{\partial T}{\partial t} + A^2 Gr\left(u\frac{\partial T}{\partial r} + \frac{1}{r}w\frac{\partial T}{\partial \theta}\right) = \frac{1}{\sigma}\left(A^2\frac{1}{r}\frac{\partial}{\partial r}\left(r\frac{\partial T}{\partial r}\right) + \frac{1}{r^2}\frac{\partial^2 T}{\partial \theta^2}\right) + \frac{1}{r\cos(A\theta)}, \tag{2.12}$$

$$\frac{1}{r}\frac{\partial}{\partial r}(ru) + \frac{1}{r}\frac{\partial w}{\partial \theta} = 0 \tag{2.13}$$

where $\gamma = ba_1/2a_2 (\approx 4.66 \times 10^{-2}$ for $T_0 = 0°\text{C})$, $\sigma = \nu/\kappa$ is the Prandtl number and all variables are now non-dimensional. The last term on the right-hand side of (2.12) is the internal heating term that drives the flow. The last terms on the right-hand sides of (2.10) and (2.11) are the buoyancy terms.

Figure 1 shows a schematic of the computational flow domain in the dimensionless coordinate system. There are extra boundaries at $r = r_{min}$ and $r = r_{max}$ that are not present in the model described in I. The boundary at $r = r_{min} > 0$ is introduced to avoid the coordinate singularity at $r = 0$ and the boundary at $r = r_{max}$ ensures that the computational domain remains finite. Most of the boundary conditions follow naturally from I:

$$T_\theta = u_\theta = w = 0 \quad \text{on} \quad \theta = 0, \tag{2.14}$$

$$T_\theta = u = w = 0 \quad \text{on} \quad \theta = -\theta_0 \equiv -\tan^{-1} A/A. \tag{2.15}$$

That is, the upper boundary $\theta = 0$ is insulated, stress free and not deformed and the lower boundary $\theta = -\theta_0$ is insulated, rigid and non-slip. Boundary conditions at $r = r_{min}$, r_{max} are derived by assuming that they are rigid and non-slip and that the temperature gradients there match those of the asymptotic solution of I:

$$u = w = 0 \quad \text{on} \quad r = r_{min}, r_{max}, \tag{2.16}$$

$$T_r = -t/(r\cos A\theta)^2 \quad \text{on} \quad r = r_{min}, r_{max}. \tag{2.17}$$

A non-slip (rather than, say, a stress free) boundary condition is chosen at $r = r_{max}$ as it more representative of what can be achieved in the laboratory. In practice, since $A \ll 1$, the influence of the boundary conditions at $r = r_{min}$ and $r = r_{max}$ on the bulk of the flow is small. Finally, the initial condition is that $u = w = T = 0$ at $t = 0$.

In terms of the dimensionless polar coordinates of the present work, the dimen-

sionless Cartesian variables used in I are

$$x = r\cos A\theta,\ z = rA^{-1}\sin A\theta, \tag{2.18}$$

$$u_{cart} = u\cos A\theta - Aw\sin A\theta \quad \text{and} \quad w_{cart} = uA^{-1}\sin A\theta + w\cos A\theta. \tag{2.19}$$

Thus at the surface $\theta = 0$ (that is $z = 0$), $x \equiv r$ and $u_{cart} \equiv u$. In the limit as $A \to 0$, $x \equiv r$, $z \equiv r\theta$, $u_{cart} \equiv u$ and $w_{cart} \equiv u\theta + w$.

3. Numerical method

The system of equations (2.10)–(2.13) is solved numerically using the method described by Armfield (1991) with appropriate adaptations to polar coordinates. Essentially, the method is a SIMPLE-type scheme applied on a non-staggered mesh with QUICK correction (Leonard 1979) for the advection terms. A detailed description of SIMPLE-type schemes can be found in Patankar (1980). The approximate pressure correction equation that is the hallmark of SIMPLE-type schemes is formulated so as to preserve ellipticity (Armfield 1991). The flow is characterized by a steep vertical front that moves through the domain. For this reason, a uniform discretization is used in the radial direction. In the tangential direction, a non-uniform grid is used to resolve boundary layers. A 226×53 grid is used here which is sufficient to ensure grid scale independence for the model parameters used in this work. The position of the left-hand boundary $r = r_{min}$ is chosen so that it is inside the diffusion-dominated flow of the tip region but is not so small as to prohibitively increase computation time. The maximum size of the time step is set by the diffusive limit for small r. The values of $r_{min} = 0.4$, $\Delta t = 5 \times 10^{-5}$ and $r_{max} = 6$ are used in the current work.

4. Results and discussion

4.1. *Introductory remarks*

Three sets of results are presented here. The first two (§§4.2 and 4.3) are motivated by the linear asymptotic theory of I. In I, it was found that the thermal bar would move out from the shallows at up to 1.5 times the speed of the associated downwelling front. The model outlined in §2 has no steady state and the asymptotic theory of I only holds for a finite time after initiation. The validity time scale depends on A^2Gr which in turn is a measure of the relative importance of the nonlinear terms in the governing equations. In the nearshore viscous-dominated flow, the constraint is $t < t_v \approx 2.1(A^2Gr)^{-1/2}$ whilst in the deeper inertia-dominated flow, the constraint is $t < t_i \approx 5.2(A^2Gr)^{-1/3}$. In §4.2, A and Gr are chosen so that the asymptotic results are valid for the duration of the simulation. This provides an opportunity to validate the asymptotic results of I.

It was suggested in I that since the thermal bar is generally ahead of the downwelling front then the circulation there would tend to move the surface signature of the thermal bar towards the shore. The results of §4.3 test to see if this occurs in practice. Thus A and Gr are chosen so that nonlinear effects are visible before the thermal bar has reached the end of the computational domain.

The final set of results (§4.4) is motivated by the experimental work of Elliott & Elliott (1969, 1970) and Kreyman (1989). As mentioned in §1, experimental observations show that the thermal bar has two stages in its propagation from the shore: an initial 'slow' and a later 'fast' stage. The asymptotic results of I and the numerical results in §§4.2 and 4.3 provide an explanation for the initial slow stage but

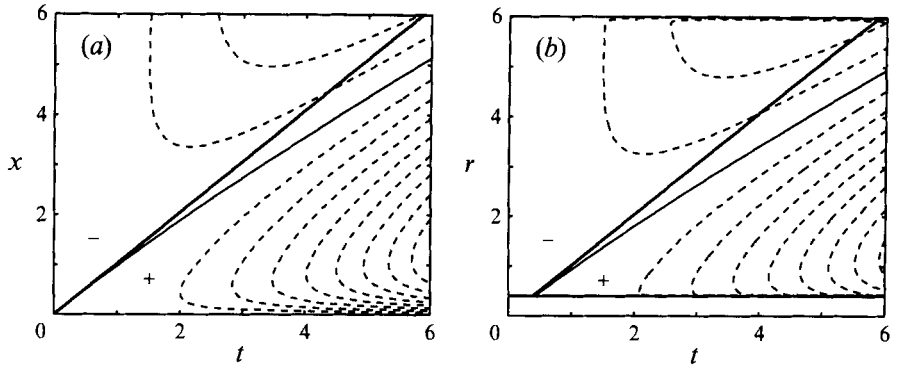

FIGURE 2. Contours of the surface velocity $u^{(0)}|_{z=0}$: (*a*) in the (t,x)-plane (from I); and (*b*) the numerical results in the (t,r)-plane for the linear case $A = 0.01$, $Gr = 500$ and $\sigma = 10$. The contour interval is 0.05 and the solid contour is the zero contour. The heavy solid line indicates the position of the thermal bar and the + and − symbols indicate the sign of the surface velocity.

not for the later fast stage. Nonlinear effects play a dominant role in the results of §4.4.

4.2. *The linear case:* $A = 0.01$, $Gr = 5 \times 10^2$

For these values of A and Gr, $t_v \approx 9$ and $t_i \approx 14$, thus the asymptotic results hold, at least while the thermal bar is still inside the computational domain. The results of this subsection provide an opportunity to validate the asymptotic results of I.

Figure 2(*a*) shows a contour plot in the (t,x)-plane of the surface velocity $u|_{z=0}$ from the asymptotic results of I. Figure 2(*b*) shows a similar set of contours but now with the numerical results (in the (t,r)-plane). The heavy line running diagonally across each plot is the surface signature of the thermal bar in each case and the solid contour is the $u|_{z=0} = 0$ contour where downwelling occurs. Overall, the agreement between the two sets of results is quite good. The main exception is near the boundaries $r = r_{min}$ and $r = r_{max}$ which are absent in the model described in I. In the numerical results, the velocity vanishes at these boundaries.

In the shallows ($x < 3$), the maximum magnitude of the numerical velocities is as much as 6.5% less than that predicted by the asymptotic results. Two effects weaken the horizontal pressure gradient in this region. The first is horizontal diffusion. The second is the tilting over of the isotherms by the flow combined with vertical diffusion. The tilting of the isotherms leads to a vertical temperature gradient that diffuses relatively rapidly leading to a lower horizontal density gradient. These effects are not included in the asymptotic analysis of I. Note that for $t > 1$, the downwelling front significantly lags the surface signature of the thermal bar. This lag is due to the time it takes for the reversal of the pressure gradient associated with the passing of the thermal bar to overcome the inertia of the existing flow. For $t < 2$, the downwelling front is in a region where the main momentum balance is between buoyancy and vertical shear so the flow reversal there occurs as soon as there is a change in sign of the pressure gradient. The downwelling front moves out slightly more slowly in the numerical results as horizontal diffusion weakens the temperature gradient, thus weakening the pressure gradient that is to reverse the flow.

Figures 3(*a*) and 3(*b*) show instantaneous streamline plots in the (x,z)-plane at $t = 5$ for the two different sets of results. In the asymptotic results, there is no vertical boundary for large x so the streamlines there are not closed. Again, the agreement between the two sets of results is quite good although the position of the dividing

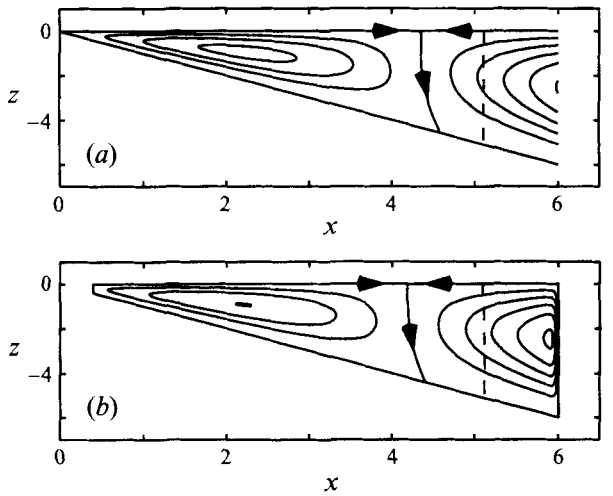

FIGURE 3. Streamline plot at $t = 5$ for (a) the asymptotic solution of I and (b) the numerical results for the linear case $A = 0.01$, $Gr = 500$ and $\sigma = 10$. The contour interval is 0.04 and the arrow heads indicate the flow direction. The dashed line indicates the position of the thermal bar.

streamline and the magnitude of the circulation differ slightly for the reasons outlined above. Note that in both cases the dividing streamline is tilted over, reflecting the three-layer velocity structure that occurs as the circulation reverses. The dashed line in figure 3 denotes the position of the thermal bar and is vertical in both cases.

4.3. *The weakly nonlinear case: $A = 0.01$: $Gr = 2 \times 10^4$*

Here, $t_v \approx 1.5$ and $t_i \approx 4.1$ so nonlinear effects will be evident before the thermal bar has reached the end of the computational domain. However the effects are not so great as to significantly disturb the circulation structure; they are apparent only in the temperature field.

Figure 4 shows contours of the surface velocity in the (t,r)-plane. As before, the heavy solid line is the surface signature of the thermal bar and the solid line is the zero contour. The dotted line indicates the position of the thermal bar according to the linear results. Overall, the results are qualitatively similar to the linear case of the previous section. However, both the thermal bar and the downwelling front move out more slowly than for the linear case. Also, the fluid velocities are generally smaller.

The smaller fluid velocities are due to the weaker pressure gradient associated with the tilting over of the isotherms by the flow and the subsequent vertical diffusion. Note that this comment refers to the non-dimensional velocities; the dimensional velocities scale with Gr which in this case is twenty times greater than that of §4.2. The tilting over of the isotherms also accounts for the thermal bar moving out more slowly than for the linear case. The circulation ahead of the downwelling front distorts the originally vertical isotherms, moving the surface signature of the thermal bar towards the downwelling front. The continual weakening of density gradients also leads to the downwelling front moving out more slowly than for the linear case. The reduction in speed is much greater for the thermal bar than it is for the downwelling front and the possibility exists that they could eventually meet as nonlinear effects increase. This does not occur in the current case but it does occur in the results of the next section. At $t \approx 5.6$, some fluid that is at the maximum density temperature emerges from the end wall at $r = 6$ and moves into the interior. This is fluid that has been carried

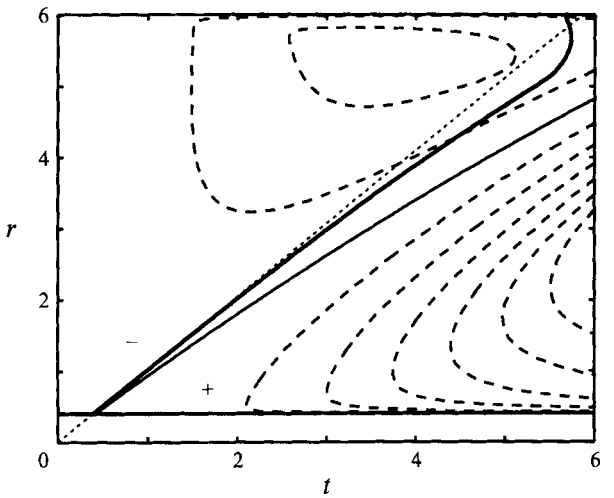

FIGURE 4. Contours of the surface velocity for the weakly nonlinear case $A = 0.01$, $Gr = 2 \times 10^4$ and $\sigma = 10$. The heavy solid line indicates the position of the thermal bar and the solid contour is the zero contour. The dotted line indicates the position of the thermal bar according to the linear results.

upwards from the depths by the strong vertical jet associated with the solid boundary at $r = 6$. This jet can be seen in figure 5 where streamlines and temperature contours at $t = 5$ are shown. In figure 5, the dashed line denotes the position of the thermal bar. Not long after $t = 5$, the thermal bar intersects the jet at $r = 6$ which quickly leads to fluid at maximum density reaching the surface. Also evident in figure 5 is the effect of the flow on the originally vertical isotherms. The circulation has distorted the isotherms so that they resemble velocity profiles. Ahead of the downwelling front, the circulation has pushed the surface signature of the thermal bar towards the shore which leads to the slower propagation speed (compared with the linear result) evident in figure 4 and discussed above. A comparison of figures 3(*b*) and 5 shows that the effect on the circulation structure is less significant.

4.4. *The nonlinear case:* $A = 0.1$, $Gr = 5 \times 10^3$

The parameter values used in this section are representative of the values realized in the experiments of Elliott & Elliott (1969, 1970) and Kreyman (1989). Kreyman reported a number of experiments with a range of different heating magnitudes and initial temperatures. Assuming molecular values of ν, Kreyman's experiments were in the range $Gr = 4000$–$57\,000$ with the vertical length scale h in the range 4.1–7.7 cm. This last range means that the tank had a non-dimensional length in the range $r_{max} = 1.9$–3.7. This is smaller than the $r_{max} = 6$ assumed in the current work, however the effect of the end wall is generally restricted to the near end region. In the present work, the vertically uniform heat source that drives the flow gives rise to larger temperature gradients (and larger velocities) than those realized in the laboratory. Thus, Gr is chosen from the lower part of the range outlined above: $Gr = 5000$. Kreyman's experimental tank had $A = 0.1$. Despite the difference in the heat input mechanism, the results presented below reproduce many of the features observed in the laboratory. For these values of A and Gr, $t_v \approx 0.3$ and $t_i \approx 1.4$ so nonlinear effects should be evident shortly after initiation.

Figure 6 is a contour plot in the (t, r)-plane of the surface velocity. As for figure 2,

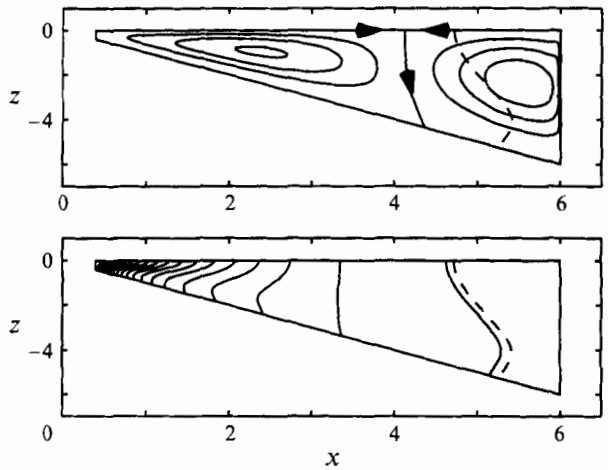

FIGURE 5. Streamlines and temperature contours at $t = 5$ for the weakly nonlinear case. The contour interval for the streamlines is 0.04 and for the temperature contours it is 0.5. The dashed line indicates the position of the thermal bar.

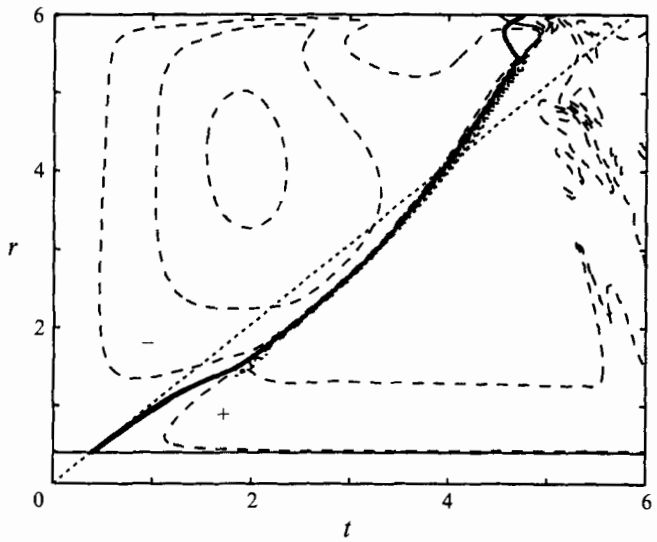

FIGURE 6. Contour plot of the surface velocity in the (t, x)-plane using the results of the nonlinear case $A = 0.1$, $Gr = 5000$ and $\sigma = 10$. The solid contour is the zero contour while the heavy solid line indicates the surface signature of the thermal bar. The contour interval is 0.02. The dotted line indicates the position of the thermal bar according to the linear results.

the solid contour is the zero contour and the heavy line (which obscures the solid contour) running diagonally across the plot is the surface signature of the thermal bar. The dotted line indicates the position of the thermal bar according to the linear results. Note that the contour interval in this figure is 0.02 whereas it is 0.05 in figure 2. The maximum (dimensionless) surface velocity in figure 2 is approximately 0.3 while in figure 6, it is approximately 0.06.

The flow development can be divided into three stages. During the initial stage ($0 < t < 1$), the results are qualitatively similar to the linear case. The thermal bar

and the downwelling front are distinct features and they each propagate out from the shallows at close to the speeds predicted by the linear results.

At $t \approx 2$, the thermal bar and the downwelling front merge to form a single feature. This signals the beginning of the second stage ($2 < t < 4$) of the flow. The merging of the two features also signals the end of the range where the asymptotic results of I provide a reasonable description of the flow. In this intermediate stage of the flow development, the thermal bar structure travels outward at a much greater speed: up to 70% faster than predicted by the linear results. During this stage, the surface velocity behind the thermal bar does not increase with time as rapidly as it does in the linear case. The flow tilts the isotherms thereby reducing the magnitude of the horizontal pressure gradient, thus there is less energy available to drive the flow.

At $t \approx 4.5$, the flow development enters its final stage where the effects of the end wall at $r = r_{max}$ are important. In this stage, the flow consists of a number of circulation cells. Also visible is fluid at the maximum density temperature ahead of the thermal bar. As will be seen later, this is fluid that was part of a gravity current that has travelled down the sloping bottom and was then carried upwards by the recirculating flow associated with the end wall. The fluid at maximum density is carried outwards by the recirculating flow over fluid of a lesser density, which is a potentially unstable configuration. The local Grashof number at $t \approx 4.5$ based on the depth and vertical density difference at $r = 5$ is $O(10^5)$. This is far in excess of the critical value $O(10^2)$ for the onset of secondary motion. This instability gives rise to the multiple-cell convection evident for $t > 4.5$. A short time after entering the final stage, the temperature is everywhere greater than that at which the density maximum occurs and the subsequent flow is of little interest in the current work. In any case, the multiple-cell convection is a consequence of the end wall which would not be present in a geophysical flow.

The three distinct stages of the flow development can be seen in figure 7 where instantaneous streamline plots and isotherms are shown for various times. The solution at $t = 1$ is representative of the initial stage of the flow where the circulation is qualitatively similar to the linear results. However the effects of advection are already evident as the temperature contours have been noticeably distorted from the vertical by the flow. Note that the dividing streamline is tilted slightly to the left as predicted by the asymptotic results of I.

By $t = 2$, the thermal bar is now a single structure with the dividing streamline and the maximum-density contour coinciding at the surface. At this time, a surface jet of warm water has started to emerge from the shallows and the isotherms are significantly tilted over in that region. At $t = 2$, the circulation magnitude is close to the maximum value that it takes during the simulation. For later times, the flow has tilted the isotherms thereby significantly reducing horizontal pressure gradients. Thus, the amount of energy available to drive a flow is reduced.

By $t = 3$, the flow development is well into the intermediate stage. The strong surface jet is carrying warm fluid out from the shallows leading to an increased propagation speed of the surface signature of the thermal bar. At the leading edge of the surface jet, there is strong downwelling and enhanced horizontal gradients. Note that the dividing streamline is now tilted over to the right which is in the opposite direction to that predicted by the asymptotic theory. Advection is now playing a dominant role in the dynamics with the result that the isotherms behind the thermal bar are nearly horizontal. This is despite the heating being vertically uniform and in contrast to the vertical isotherms of the asymptotic solution of I.

Another feature of the intermediate stage is a gravity current consisting of fluid at

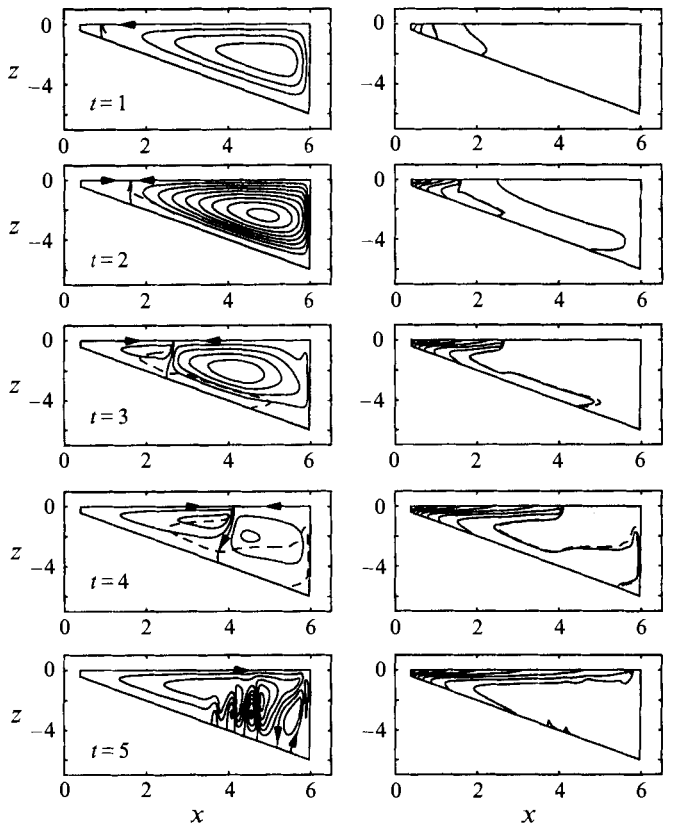

FIGURE 7. Streamline and temperature contours at a various times from the results of the nonlinear case. The dashed line in each plot indicates the position of the thermal bar. The contour intervals are 0.01 for the streamfunction and 0.5 for the temperature plots.

close to maximum density travelling down the sloping bottom. This gravity current advances much more rapidly than the surface jet owing to the favourable circulation ahead of the thermal bar as well as the extra acceleration associated with the sloping bottom. The gravity current and the warm surface jet combine to yield a complicated structure for the thermal bar. This makes it difficult to define the 'position' $x(t)$ of the thermal bar in a consistent way.

At $t = 4$ the flow development is near the end of the intermediate stage. The surface jet is still advancing though it is slightly deeper than it was at $t = 3$. The surface jet is deepening much more slowly than the topography and at $t = 4$ is occupying approximately 25% of the total depth at its head. The dividing streamline has tilted further over to the right as the warm surface jet progresses. The gravity current has now travelled the entire length of the domain and is being carried up to the surface by the anti-clockwise circulation ahead of the thermal bar.

The circulation and temperature structure at $t = 5$ is representative of the final stage of the flow where there are multiple circulation cells and the fluid is everywhere warmer than the temperature at which the density maximum occurs. Since the density is now a monotonic function of the temperature, the subsequent flow is of little interest in the present work. In any case, there are features present that have relatively few grid points to resolve them and it is not reasonable to suppose that the results for $t > 5$ are grid-scale independent.

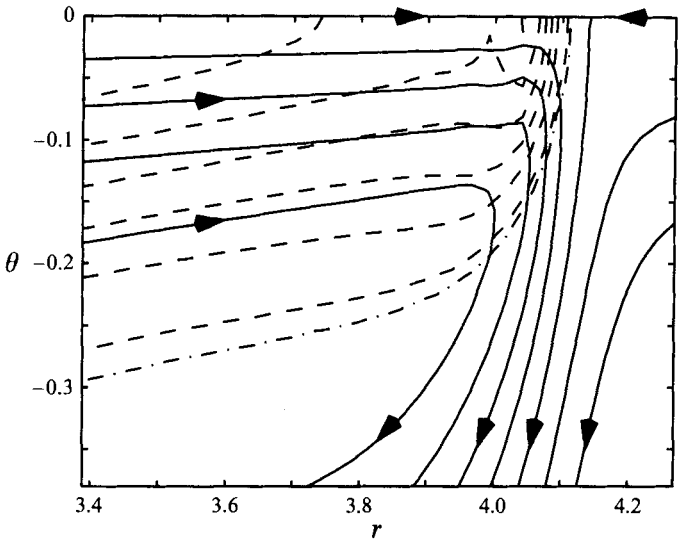

FIGURE 8. Detail of the leading edge of the warm surface jet at $t = 4$. The dashed lines are temperature contours and the solid lines are streamlines. The dot-dash line indicates the position of the thermal bar. The contour intervals for the temperature and streamfunction are 0.25 and 0.005 respectively.

Figure 8 shows a detail of the leading edge of the warm surface jet at $t = 4$. Just behind the leading edge, the converging flow has set up strong horizontal temperature gradients. Note however that the corresponding density gradients are relatively weak since the density is a weak function of temperature close to the density maximum. The strong gradients all occur to the left of the density-maximum contour which acts as a strong barrier to horizontal transport. It has already been noted that the advection velocity behind the thermal bar is greater than its propagation speed. The flow that is in excess to the propagation is directed downwards as a narrow sinking jet. This type of feature has been observed by Ivey & Hamblin (1989) in their laboratory study of convection of water close to the density maximum. In dimensional terms, the ratio of the fluid velocities immediately behind the head of the surface jet and the propagation speed is approximately two to one. Thus a comparison between the present moving downwelling region and the stationary front in Ivey & Hamblin's experiments can only be qualitative. A feature of the sinking jet is the overshoot of the isotherms as the warm surface fluid is carried downwards. This overshoot is also a characteristic of the sinking jets observed by Ivey & Hamblin. It is clear from figure 8 that the maximum-density contour and the dividing streamline do not precisely coincide. This must be the case if advection is to contribute to the propagation of the thermal bar; streamlines must cross the maximum-density contour for the flow to carry it forward.

The structure of the sinking region at the head of the surface jet is reminiscent of the sinking plume considered by Kay *et al.* (1995) in their boundary layer analysis of the thermal bar. The main difference is that the structure in the present results is highly non-symmetric with very small temperature gradients to the right of the thermal bar. Given this difference and the unsteady nature of the results, it is not clear how the results of Kay *et al.* can be applied to the present case except to note that the concentrated isotherms and streamlines resemble a boundary layer structure.

The non-dimensional radial (horizontal) advective heat transfer per unit width

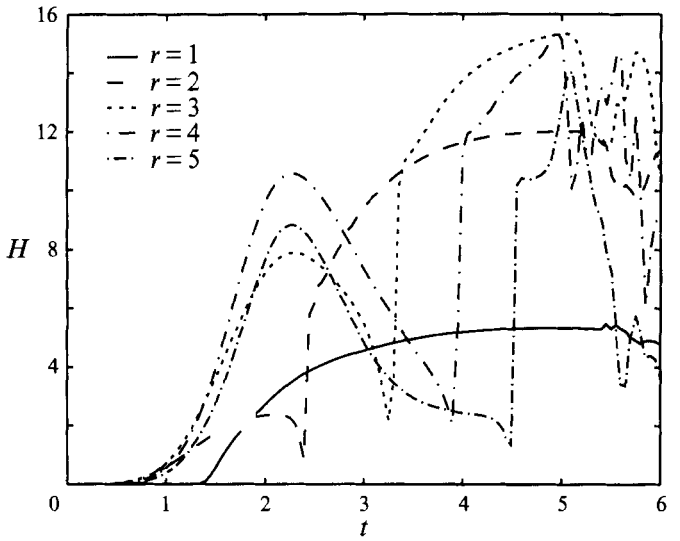

FIGURE 9. Time series of the radial advective heat transfer H at a number of different values of r for the nonlinear case.

across a section located at r =constant is

$$H = AGr\, r \int_{-\theta_0}^{0} uT \, \mathrm{d}\theta. \tag{4.1}$$

The heat transfer has been non-dimensionalized by hI_0 Wm^{-1}. The total heat transfer includes a conductive component but this is several orders of magnitude smaller than the advective component and is thus not discussed here. Note that for H to be non-zero, there must be some vertical structure in the temperature otherwise $H = 0$ by virtue of conservation of mass. Figure 9 shows a times series of H at a number of different values of r. Note that $H > 0$ for all times both before and after the thermal bar has passed a particular station. Ahead of the thermal bar, the circulation is generally anti-clockwise. This carries warm fluid down the slope and cooler water towards the tip at the surface. This yields a net transfer of heat to the right. Behind the thermal bar, the circulation is generally clockwise with a warm surface outflow which again yields a net positive heat flux.

At each station, H is small until $t \approx 1$ by which time advection has set up a significant thermal stratification both behind and ahead of the thermal bar. The heat transport then rises as the circulation and stratification strengthen. Eventually, the approaching thermal bar weakens the circulation and the heat transfer starts to drop. Note that the maximum H before the arrival of the thermal bar occurs at approximately the same time of $t \approx 2$ at all stations except $r = 1$. As a function of t, the surface velocity is at its greatest near $t = 2$ at all stations except $r = 1$ (see figure 6). The drop in the heat transfer reflects the decreasing magnitude of the circulation. At $r = 1$, there is no local maximum of the surface velocity near $t = 2$ though it appears to approach a finite maximum as t increases. This is reflected in the behaviour of the advective heat transfer at $r = 1$. The heat transfer reaches a maximum as the flow and temperature reach a quasi-steady state where the horizontal advection of heat is balanced by vertical diffusion. The vertically averaged temperature continues to increase but the vertical and horizontal gradients achieve a steady state, as does the circulation.

The arrival of the warm surface jet at stations $r = 2$, 3, 4 and 5 causes a sharp increase in H. In fact, the local minimum that precedes this increase is a good indicator of the arrival time of the surface jet. This sudden jump is not surprising given the large temperature gradients associated with the leading edge of the surface jet (see figure 8). For times greater than $t \approx 5$, the time series at each station become quite erratic as the circulation structure breaks up into many cells. As was noted earlier, the results for $t > 5$ are not necessarily independent of the grid scale and so interpretation of the behaviour of H for these later times is difficult.

A comparison of the results of this simulation with available experimental data is necessarily largely qualitative. As has already been noted, the heat input mechanism assumed in the current work is significantly different from that of the laboratory work of Elliott & Elliott (1969, 1970) and Kreyman (1989). Despite this, the current results capture some of the important features of the experimental work. The dimensionless length of the experimental tank used by Kreyman was in the range $l = 2$–4. This means that the present results are relevant up to $t \approx 4$ after which time the thermal bar is outside the experimental domain.

Despite the vertically uniform heat source, the present results include a strongly stratified region in the shallows behind the thermal bar. In the present results, the stratified region is set up by advection. The stratification behind the thermal bar is much more pronounced than it is in the deeper parts which is consistent with both experimental and field observations though they may arise via different mechanisms. In fact, the stratification in the shallows is much stronger in the present results than it is in the experimental results of Kreyman (1989) or Elliott & Elliott (1969, 1970). In dimensional terms, a typical vertical temperature difference is 6–8° in the present results whereas it is 4–5° in Kreyman's results and 2–3° in Elliott & Elliott's. This is due to the initially much larger temperature differences that occur in the vertically integrated heat input model considered here.

A consequence of the larger temperature gradients is larger fluid velocities. The maximum velocity observed by Kreyman (1989) was $\approx 10^{-4}\mathrm{m\,s^{-1}}$. The maximum velocity predicted by the numerical results is $\approx 2 \times 10^{-4}\mathrm{m\,s^{-1}}$. This is despite Gr being chosen from the lower end of the range achieved in the experiments. The larger velocities in the numerical results suggests that advection might be more significant in the present results than in Kreyman's experiments.

Kreyman (1989) and Elliott & Elliott (1970) noted that some time after the initiation of their experiments, the propagation speed of the thermal bar suddenly increased. In fact they found that for small times, the propagation speed is less than that predicted by a purely heat-balance-based estimate. For larger times, the speed is greater than that based on the same prediction. A similar increase in propagation speed occurs in the present results at a non-dimensional time of $t \approx 2$ which is consistent with the times observed by Kreyman and Elliott & Elliott. The mechanism that gives rise to this increase in speed is now clear; it is via the formation of a warm surface jet emanating from the shallows with a depth at its head less than the local fluid depth. The advancing surface jet is fed by warm water from the shallows and there is strong downwelling at its head.

5. Concluding remarks

The model considered in this paper is a considerable simplification of the thermal bar phenomenon. The most striking simplification is the use of a vertically uniform heat source to drive the model. Despite this, when nonlinear effects are important, the

model produces many of the features observed in laboratory models of the thermal bar. These include a strongly stratified region in the shallows and an initial 'slow' and then a 'fast' propagation speed of the thermal bar.

Including different heat input mechanisms in a numerical model is fairly straightforward. However, accurate and systematic modelling of heating mechanisms that operate in a real lake is difficult and beyond the scope of this paper. For example, Rodgers (1968) noted that the penetration depth of solar radiation varied considerably across the thermal bar. Also, the heat flux at the surface due to sensible and latent heat transfer both in the field and the laboratory is difficult to quantify.

It appears, in the non-rotating case considered here, that the propagation of the thermal bar is governed by the conditions at the head of the warm surface jet that emanates from the shallows. Perhaps a boundary layer analysis similar to that of Kay *et al.* (1995) that takes into account propagation and unsteadiness could provide some insight into the propagation mechanism. Coriolis effects would also modify the propagation of the jet as well as the overall circulation structure.

The author gratefully acknowledges the many suggestions for improvement made by S. Brown and the anonymous reviewers on earlier versions of this paper.

REFERENCES

ARMFIELD, S. W. 1991 Finite-difference solutions of the Navier-Stokes equations on staggered and non-staggered grids. *Computers Fluids* **20**, 1–17.

BENNETT, J. R. 1971 Thermally driven lake currents during the spring and fall transition periods. In *Proc. 14th Conf. Great Lakes Res.* pp. 535–544. Intl Assoc. Great Lakes Res.

ELLIOTT, G. H. 1970 A mathematical study of the thermal bar. In *Proc. 13th Conf. Great Lakes Res.* pp. 545–554. Intl Assoc. Great Lakes Res.

ELLIOTT, G. H. & ELLIOTT, J. A. 1969 Small-scale model of the 'thermal bar'. In *Proc. 12th Conf. Great Lakes Res.* pp. 553–557. Intl Assoc. Great Lakes Res.

ELLIOTT, G. H. & ELLIOTT, J. A. 1970 Laboratory studies on the thermal bar. In *Proc. 13th Conf. Great Lakes Res.* pp. 413–418. Intl Assoc. Great Lakes Res.

FARROW, D. E. 1995 An asymptotic model of the hydrodynamics of the thermal bar. *J. Fluid Mech.* **289**, 129–140 (referred to herein as I).

GEBHART, B., JALURIA, Y., MAHAJAN, R. L. & SAMMAKIA, B. 1988 *Buoyancy-Induced Flows and Transport*. Hemisphere.

HUANG, J. C. K. 1972 The thermal bar. *Geophys. Fluid Dyn.* **3**, 1–28.

HUBBARD, D. W. & SPAIN, J. S. 1973 The structure of the early spring thermal bar in Lake Superior. In *Proc. 16th Conf. Great Lakes Res.* pp. 735–742. Intl Assoc. Great Lakes Res.

IVEY, G. N. & HAMBLIN, P. F. 1989 Convection near the temperature of maximum density for high Rayleigh number, low aspect ratio, rectangular cavities. *Trans. ASME* C: *J. Heat Transfer* **111**, 100–105.

KAY, A., KUIKEN, H. K. & MERKIN, J. H. 1995 Boundary-layer analysis of the thermal bar. *J. Fluid Mech.* **303**, 253–278.

KREYMAN, K. D. 1989 Thermal bar based on laboratory experiments. *Oceanology* **29**, 695–697.

LEONARD, B. P. 1979 A stable and accurate convective modelling procedure based on quadratic upstream interpolation. *Comput. Meth. Appl. Mech. Engng* **19**, 59–98.

MALM, J. 1994 Thermal bar dynamics; spring thermo- and hydrodynamics in large temperate lakes. PhD thesis, Lund University, Sweden.

MALM, J., GRAHN, L., MIRONOV, D. & TERZHEVIK, A. 1993 Field investigation of the thermal bar in Lake Ladoga, spring 1991. *Nordic Hydrology* **24**, 339–358.

MALM, J., MIRONOV, D., TERZHEVIK, A. & JÖNSSON, L. 1994 Investigation of the spring thermal regime in Lake Ladoga using field and satellite data. *Limnol. Oceanogr.* **39**, 1333–1348.

MALM, J. & ZILITINKEVICH, S. S. 1994 Temperature distribution and current system in a convectively mixed lake. *Boundary Layer Met.* **71**, 219–234.

PATANKAR, S. V. 1980 *Numerical Heat Transfer and Fluid Flow*. Hemisphere.

RODGERS, G. K. 1968 Heat advection within Lake Ontario in spring and surface water transparency associated with the thermal bar. In *Proc. 11th Conf. Great Lakes Res.* pp. 942–950. Intl Assoc. Great Lakes Res.

ZILITINKEVICH, S. S. KREIMAN, K. D. & TERZHEVIK, A. YU. 1992 The thermal bar. *J. Fluid Mech.* **236**, 27–42.